A novel semi-empirical approach to non-destructively evaluate the effect of infills on frame buildings

José Barros[c,b,*], Manuel Chiachío[a,b], Leandro Morillas[b], Wilson Torres[d], David Suco[c]

[a] *Andalusian Research Institute in Data Science and Computational Intelligence, University of Granada, 18071 Granada, Spain*
[b] *Dept. Structural Mechanics & Hydraulics Engineering, University of Granada, 18071 Granada, Spain*
[c] *Faculty of Engineering, Catholic University of Santiago de Guayaquil, Guayaquil, Ecuador*
[d] *Department of Civil Engineering, Universidad de La Frontera, Francisco Salazar Ave. 01145, Temuco, Chile*

Abstract

Masonry infilled frame (MIF) structures are commonly used as building system in many regions, and particularly in Latin American, Mediterranean, and Pacific countries, which are areas highly exposed to seismic events. It is well known that the influence of the infilled frames on the seismic response is affected by several sources of uncertainties which create unsafe unaccuracies in the seismic behaviour of a building. The use of existing complex models is an option which require a large number of specialized input values and data mostly obtained from in-situ destructive tests, thus making them infeasible in many practical cases. This research is a first attempt to provide an approach which provides prediction of the structural behaviour of a MIF with quantified uncertainty, and using as inputs values that can be obtained through a low-cost non-destructive test. The proposed method exploits the known interaction between the in-plane (IP) and out-of-plane (OoP) behaviour of the masonry wall by providing a semi-empirical model which predicts the IP stiffness of the MIF in terms of the measured OoP fundamental frequency. The semi-empirical approach has been nurtured with five experimental tests over one-fourth scale MIFs, where the OoP fundamental frequency variation has been obtained in terms of the IP deformation history. The results indicate that the proposed method can become a practical tool to experimentally quantify the contribution of the masonry infills of existing frame buildings, and also to theoretically predict it during design phase. However, a larger dataset of tests should be used on the calibration of the method before its application in real cases.

Keywords: Masonry Infilled Frames, Approximate Bayesian Computation, Seismic Design, Non-Destructive Tests

Nomenclature

*Corresponding author. e-mail: jose.barros@cu.ucsg.edu.ec

f_c, f_{cu}	Constitutive values of the maximum and ultimate concrete strength in the reinforced concrete frame model applied to the parametric study model.
$f_{f'_m}$	Modifier factor of the equivalent strut stiffness due to masonry characteristic compressive strength.
$f_{H/L}$	Modifier factor of the equivalent strut stiffness due to height/length ratio.
$f_{H/t}$	Modifier factor of the equivalent strut stiffness due to height/thickness ratio.
f_m	Characteristic compressive strength of the masonry wall.
f_{OoP}	Out of plane natural frequency of the masonry wall.
f_{scale}	Modifier factor of the equivalent strut stiffness due to scaling factor.
f_y, E_s, b	Yield strength, elastic modulus and strain hardening ratio parameters to define the constitutive behaviour of the reinforcing steel in the reinforced concrete frame model applied to the parametric study model.
k_0	Out of plane stiffness of the masonry wall under undamaged condition.
k_i	Out of plane stiffness of the masonry wall under previous damaged condition.
k_{IP}	In plane stiffness of the masonry wall.
t OR t_m	Thickness of the masonry wall.
w_m	Width of the masonry wall macro-model equivalent strut.
A, B	Uncertain model parameters to derive the proposed formulation.
A_m	Area of the masonry wall macro-model equivalent strut.
C, D	Uncertain model parameters to derive the proposed formulation.
D_1, D_2, β	Parameters to account for degradation due to cyclic deformation in the strain penetration model applied into the reinforced concrete frame non-linear model of the parametric study.
E, F	Uncertain model parameters to derive the proposed formulation.
E_c, E_m	Elastic moduli of the materials of the proposed model, which compose the frame and the equivalent strut, respectively.
E_m	Elastic module of the masonry wall.
F_0	Out of plane strength of the masonry wall under undamaged condition.
F_i	Out of plane strength of the masonry wall under previous damaged condition.
H OR H_m	Height of the masonry wall.
I_c, I_v	Gross inertia of the columns and beam, respectively, of the frame in the proposed model.
L OR L_m	Length of the masonry wall.
M_1, M_2	Constitutive values of the flexure behaviour of the strain penetration model applied into the reinforced concrete frame non-linear model of the parametric study.
$Pinch_x$	Parameters to account for strain pinching effect in the strain penetration model applied into the reinforced concrete frame non-linear model of the parametric study.
$Pinch_y$	Parameters to account for stress pinching effect in the strain penetration model applied into the reinforced concrete frame non-linear model of the parametric study.
R_k	Relation of the stiffness reduction in the out of plane direction due to an in plane inter-story drift deformation.
R_F	Relation of the strength reduction in the out of plane direction due to an in plane inter-story drift deformation.
δ	In plane deformation of the masonry infilled wall.
ϵ_c, ϵ_u	Constitutive values of the strain corresponding to the maximum and ultimate concrete strength in the reinforced concrete frame model applied to the parametric study model.
$\theta_1 \dots \theta_5$	Calibration parameters of the proposed method.

θ_1^{rot}, θ_2^{rot}	Constitutive values of the rotational deformation behaviour of the strain penetration model applied into the reinforced concrete frame non-linear model of the parametric study.
IP	In plane.
ISD	Inter-story drift.
MIF	Masonry infilled frame.
OoP	Out of plane.
PDS	Power density spectrum.

1. Introduction

Frames with unreinforced masonry infills are encountered as structural systems commonly used worldwide. There are regions, like in Guayaquil-Ecuador, where the reinforced concrete frames with unreinforced masonry infills represent about the 75% of the total amount of building structures, according to [5]. Similar conditions are found in other regions of Ecuador and beyond [40, 80, 86–88]. These infills are usually neglected in the structural analysis and design in common building engineering practice, mostly because of insufficient provisions of different national design standards [42] and lack of tested knowledge about their contribution to the building response as structural components [2]. Therefore, a better understanding of the structural contribution of the infills is a need for the development of risk-reduction programs, overall in regions severely affected by seismic events.

In the literature, several approaches have been proposed to model the behaviour of the masonry infilled frames (MIFs), and they can be typically classified as *micro*, *meso* and *macro* modelling approaches [61, 82]. Authors like Sattar and Liel [78] [79] proposed the application of a *strut* model enhanced by the use of micro-modelling for the seismic evaluation of MIF buildings. Most of these models only consider the IP behaviour of the structural system [37, 46, 77]. A literature review of available IP stiffness estimate formulations is shown in Table 1, for the elastic range behaviour (both tangent and secant stiffness formulations are presented), which are usually applied for design purposes. Other authors have proposed more comprehensive models that are able to account for the interaction between the IP and OoP behaviour. A literature review of the available models is listed in Table 2. Among them, some micro-models are able to capture such interaction directly. However, the micro-models require a big amount of input data usually not available for existing structures, thus limiting their applicability. On the other hand, current reference standards for the seismic evaluation of existing buildings, like the ASCE/41-17 [6], stipulate the need to "validate the use of finite element models and strut models by considering published or project specific experimental data from cyclic *quasi-static* or dynamic tests" for the MIF structural systems, due to their complex behaviour and the uncertainties affecting their response. These uncertainties are related to a number of factors such as: (1) the

variety of masonry material types used; (2) the uncertainty in their mechanical characteristics (like strength, geometry, void directions, void to fill ratios, among others); (3) the human-factor influence, mostly during construction phase [82]; and (4) the insufficiently known frame-infill interactions [13, 60]. Some authors have made successful attempts to better estimate the uncertainty about these influencing factors through a detailed characterization of the MIFs by a number of destructive tests [27, 52]. However, these tests produce considerable increase of building costs when applied during the design or construction phase, which are unfeasible overall for small and medium size structures, and are infeasible for existing buildings due to the damage produced to the structure (even when moderately destructive tests are used [52]). This problem reveals the need of a practical method, based on non-destructive tests, for the evaluation of existing buildings made of MIFs, that can be easily applied in-situ and without the need of complex, yet expensive, equipment. This paper is a first attempt in this direction.

Table 1: IP equivalent strut macro-modelling of MIF - main contributions

Reference	**Strength**	**Deformation**	**Stiffness**
[37][a]	-	-	$K_e = E_m t_m \left[0.318\,(\lambda H_m)^{-0.661}\left(\frac{H_m}{L_m}\right)^{-0.871}\right]$
[37][b]	-	-	$K_e = 0.0143 E_m^{0.618} t_m^{0.694}\left(\frac{H_m}{L_m}\right)^{-1.096}$
[46][a]	$0.85V_p$	$d_{85} = 0.0013H_m$	$K_e = \frac{0.85V_p}{d_{85}}$
[46][b]	$0.40V_p$	$d_{40} = 0.00025H_m$	$K_e = \frac{0.40V_p}{d_{40}}$
[77][a]	-	-	$K_e = E_m t_m \left[0.175\,(\lambda H_m)^{-0.4}\right]$
[77][b]	-	-	$K_e = \frac{G_m L_m t_m}{H_m}$

[a]Basic formulation for secant stiffness of the equivalent strut.
[b]Basic formulation for initial stiffness of the equivalent strut.

Table 2: OoP modelling of MIF - main contributions

Reference	**Theory / modelling criterium**	**Observations**
[85]	Timoshenko beam action considering linear, elastic, homogeneous and isotropic material	Only OoP behaviour
[25, 31, 32, 35, 36]	Yield line analysis considering two way action	Only OoP behaviour
[53, 54, 63, 84, 89]	One way arching action	Only OoP behaviour
[9, 19, 43, 45]	Virtual work principle, two way arching action	Only OoP behaviour
[4, 30, 72]	One way arching action	IP history considered
[33, 34]	Macro-modelling: 3D compression only struts with a concentrated mass in the center	IP -OoP interaction directly considered
[23, 39, 66]	Macro-modelling: Fiber section strut model with a concentrated mass in the center	IP -OoP interaction directly considered
[16, 22, 28, 64, 75, 76]	Macro-modelling: Empirical reduction factor in terms of IP deformation history	IP history considered
[11, 24, 44, 49, 62, 67, 90]	Micro-modelling: Concrete damage plasticity model	IP -OoP interaction directly considered
[7, 47, 48]	Micro-modelling: Drucker Prager model	IP -OoP interaction directly considered
[73]	Meso-modelling: Multi-pier model	IP -OoP interaction directly considered

Indeed, this paper proposes a non-destructive non-invasive semi-empirical approach to estimate the in-plane (IP) stiffness of the MIF through the out-of-plane (OoP) dynamical response of the walls. This IP-OoP interaction has been experimentally observed in several studies [3, 14, 16, 17, 21, 22, 55–59, 68, 71],

where it was demonstrated that the OoP stiffness and strength of the wall are reduced in proportion to the maximum IP deformation it has been subjected to. Table 3 summarizes some of the laboratory tests results available in the literature where the MIFs were subjected to IP deformation before applying OoP force until collapse, where the maximum IP inter-story drift (IP ISD) is compared to the following parameters:

$$R_F = \frac{F_i}{F_0} \tag{1}$$

$$R_k = \frac{k_i}{k_0} \tag{2}$$

where F_i and k_i are the OoP strength and stiffness, respectively, of the MIF that was subjected to an IP ISD before the OoP test (i.e damaged condition), and F_0 and k_0 are the OoP strength and stiffness, respectively, of a reference MIF specimen that was not subjected to any level of IP ISD before the OoP test (i.e undamaged condition). Figure 1 demonstrates that the history of IP deformation reduces the OoP strength and stiffness of the wall.

Table 3: Literature review of OoP tests of MIFs that were previously subjected to IP deformations.

Author	**L** (m)	**H** (m)	**t** (mm)	**IP ISD** (%)	$\mathbf{R_F}$	$\mathbf{R_k}$
Ricci et al. [75]	2.350	1.830	80	0.16	1.06	0.84
	2.350	1.830	80	0.37	0.48	0.08
	2.350	1.830	80	0.58	0.27	0.06
	2.350	1.830	120	0.21	0.99	0.82
	2.350	1.830	120	0.50	0.67	0.21
	2.350	1.830	120	0.89	0.55	0.14
Angel et al. [4]	2.440	1.625	48	0.22	0.76	0.53
	2.440	1.625	48	0.34	0.51	0.51
Calvi and Bolognini [16]	4.200	2.750	135	0.40	0.27	0.08
	4.200	2.750	135	1.20	0.18	-
Furtado et al. [28]	4.200	2.300	150	0.50	0.26	-
De Risi et al. [21]	1.830	1.830	80	0.15	1.07	0.61
	1.830	1.830	80	0.28	0.76	0.35
	1.830	1.830	80	0.51	0.65	0.22

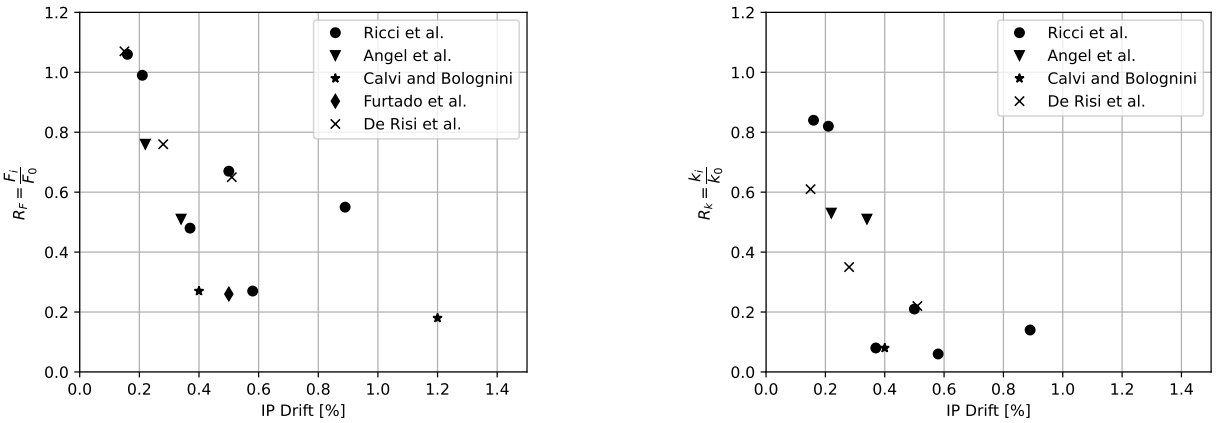

Figure 1: Influence of IP deformation history on the OoP strength (left) and stiffness (right) of a MIF wall, according to experimental evidence gathered by several authors.

The method presented here gives the IP stiffness of a MIF using a parameterized semi-empirical model whose parameters are inferred from batch sequences of IP-OoP data experimentally obtained at increasing levels of IP horizontal drifts. The novelty of the method resides in the fact that it only needs the OoP fundamental frequency of the wall as input parameter, which can be obtained by non-destructive non-complex testing using well-known system identification methods [74]. Several authors have used system identification to obtain the frequency and modal shapes of existing walls in the out-of-plane direction to characterize their dynamic behavior. Table 4 shows a summary of the tests performed by several authors and their results. However, to the authors knowledge, identification of natural frequencies have not been done yet on MIF walls subjected to controlled levels of IP drifts. A dedicated experimental campaign has been carried-out to ensure that the model, once inferred using the data, can produce predictions within a wide range of MIF configurations and loading cases. For model inference, a Bayesian prediction and updating framework is used to properly tackle with the inherent uncertainty of the problem. Besides, and because an unlimited experimental dataset convering all possible MIF configurations is impossible, a meso-model based approach is used to enrich the proposed model and to extend it to MIF configurations out of the range covered by the tested data. The proposed method has been applied to produce IP stiffness predictions of four MIFs with quantified uncertainty with satisfactory results in terms of precision and accuracy. The results indicate that the proposed method is efficient to non-destructively evaluate the contribution of the masonry infills for existing buildings.

The remaining of the paper is organized as follows. Section 2 describes the experimental campaign carried out during this investigation and provides characterization of the measurements. Section 3 gives the basis and main assumptions about the proposed IP-OoP model of the structural MIFs, along with its model parameterization. In Section 4, the problem of model inference is formulated using an Approximate Bayesian Computation inverse problem framework. This section also gives the corresponding computational issues

Table 4: Literature review of MIF wall system identification of the fundamental OoP frequency

Author **Frame / Wall materials**	**Specimen**	**t** (mm)	**Openings**	**L x H** (m)	**Plaster**	**IP damage**	**OoP freq.** Hz)
Nicoletti et al. [70]	W1-A	300	No	-	No	No	65.55
- RC frames		300	No	-	Yes	No	90.43
- Hollow clay bricks	W2-A	120	No	-	No	No	49.70
		120	No	-	Yes	No	64.31
	W3-A	80	No	-	No	No	21.87
		80	No	-	Yes	No	34.24
De Angelis and Pecce [20]	1	120	No	5.10x3.48	Yes	No	18.43
- RC frames							
- Hollow clay bricks							
Furtado et al. [29]	A1	110	No	3.50x1.30	No	No	31.70
- RC frames	A2	110	No	3.50x1.30	No	No	24.50
- Hollow clay bricks	A3	110	No	3.55x3.20	No	No	16.50
	A4	110	No	3.20x0.95	No	No	22.40
	A5	110	No	3.55x3.20	No	No	30.00
	A6	110	Door	2.75x3.20	No	No	22.50
	A7	110	Door	2.45x3.20	No	No	22.70
	A8	150	No	5.00x1.75	No	No	18.00
	A9	150	No	2.75x2.30	No	No	34.20
	A10	110	No	3.60x1.00	No	No	34.10
	A11	220	Window	3.20x2.80	No	No	11.50
	A12	220	No	3.40x2.80	No	No	28.20
	A13	220	No	3.70x2.80	No	No	27.60
	A14	110	No	2.10x3.20	No	No	14.70
	B1	110	No	3.90x2.70	No	No	22.40
	B2	110	Window	3.80x2.70	No	No	18.20
	B3	110	No	3.50x2.70	No	No	27.30
	C1	80	Window	3.15x2.55	No	No	53.57
	C1	150	Window	3.15x2.55	No	No	53.48
	C2	110	Door	3.05x2.55	No	No	64.45
	C2	150	Door	3.05x2.55	No	No	57.13
	C3	110	No	3.50x2.80	No	No	31.56
Varum et al. [87]	Wall 1	-	No	3.90x2.20	Yes	No	31.83
- RC frames	Wall 2	-	No	2.70x2.20	Yes	No	46.43
- Hollow and solid clay bricks	Wall 3	-	Window	3.90x2.20	Yes	No	10.00
	E12D Wall1	-	No	1.60x2.60	Yes	No	53.49
	E12D Wall2	-	No	1.60x2.60	Yes	Yes	35.74
	E12D Wall3	-	No	3.10x2.60	Yes	No	44.03
	E12D Wall4	-	No	3.10x2.60	Yes	Yes	20.41
Nicoletti et al. [69]	Wall 1a	60	No	4.00x2.75	No	No	16.80
- Steel frame	Wall 1b	60	No	4.00x2.76	Yes	No	17.30
- Hollow clay bricks	Wall 2a	60	No	4.00x2.77	No	No	17.90
	Wall 2b	60	No	4.00x2.78	Yes	No	18.10
	WE1	250	No	2.00x2.84	Yes	No	64.73
	WI1	120	No	2.10x2.84	Yes	No	41.81
	WI2	80	No	3.45x2.84	Yes	No	22.10

that must be addressed for our needs. The results are presented in Section 5, followed by a discussion of the results in Section 6 through a parametric study that includes the variability of parameters not covered within the experimental campaign. Finally, Section 7 gives concluding remarks.

2. Description of experimental research

This section provides the description of the experimental tests along with characterization of their results.

2.1. Description of the specimens

In this work, five one-fourth scale, one-bay one-story masonry infilled frames were tested, as shown in Figure 2. Additionally, two specimens (metallic and concrete, respectively) of frames without walls, were tested for comparative purposes. Among the infilled frames, three specimens consisted of reinforced concrete

frames whereas the remaining two were made of structural steel. The infill walls were built with hollow concrete masonry units of 100x50x50 mm, bonded with a ready-mixed N-type mortar, covering a wall of 750 mm clear height, and $\{500, 750, 1000\}$ mm clear bay, for the three concrete frames; and $\{500, 1000\}$ mm, for the steel ones, respectively. Concrete columns were 75x75 mm cross section with longitudinal reinforcement ratio of 0.024 (i.e. four 6.5 mm diameter bars) and 10 mm of cover. Their transverse reinforcement consisted on one 3.5 mm diameter stirrup with 18 mm separation. Shear connection between the wall and the columns is enhanced by installing three 3.5 mm diameter bars equally separated along the height of the columns, and properly anchored in both the column and the wall, in coincidence with a joint mortar bed. Top beam was designed with 62.5x87.5 mm cross section using two 5.5 mm and 4.5 mm bars, as top and bottom reinforcements, respectively. No special connection was made between the wall and the top beam, only a mortar bed was placed. Beam transverse reinforcements consisted on one 2.5 mm diameter stirrup every 18 mm of separation. For the steel frames, HSS was used for the columns using 75x75x3 mm as cross section, whereas an IPN-100 was employed for the beam. The geometric and building details for both, the concrete and steel structural sections, are shown in Figure 3. Also, note from Figure 2 that, a 250x250 mm reinforced concrete beam with four 18 mm diameter longitudinal reinforcing bars and 5.5@150 mm stirrups, was used in all the specimens as bottom beam. This beam was anchored to the reaction frame with two 24 mm bars, as shown in Figure 4. The mechanical properties of the materials used for the specimens described above, are shown in Table 5.

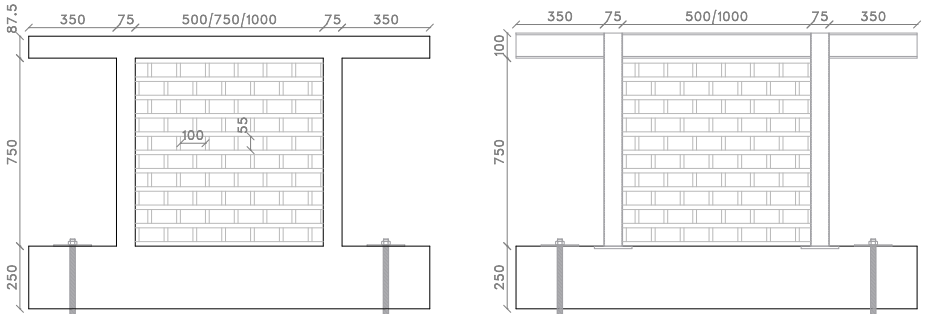

Figure 2: General geometric characteristics of the masonry infilled concrete and steel frame specimens.

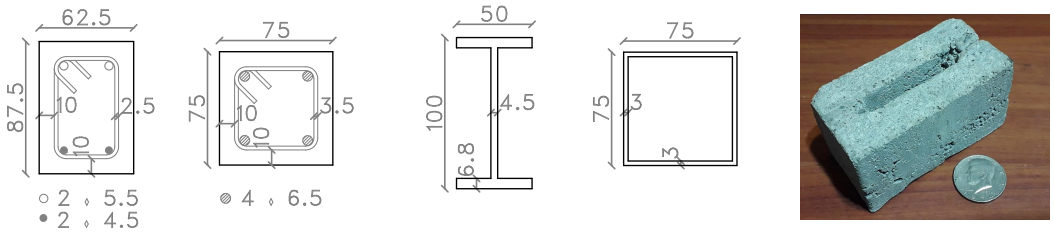

Figure 3: Geometric and building details of the concrete and steel beam and column sections, and masonry unit used in the specimens.

Table 5: Mechanical properties of the materials used for the test specimens.

Element	Test	Mean Value (MPa)	Std. Deviation (Mpa)
Mortar	Flexure	3.74	0.28
	Compression	10.04	0.40
Masonry unit	Compression	9.54	0.25
Wall	Diagonal tension	1.16	0.05
	Compression	2.64	0.21
Steel Reinforcement[a]:			
3.5 mm	Yield tension	441.7	
4.5 mm	Yield tension	466.3	
5.5 mm	Yield tension	568.8	
7.5 mm	Yield tension	699.6	

[a]Only one coupon was tested for each size of steel reinforcement.

2.2. Test procedure

The test procedure designed in this work is described next. First, each masonry infilled frame was anchored to the rigid frame. To experimentally model the lateral OoP restriction induced by an upper floor slab, the top beam was laterally restrained against OoP displacements using an ensemble of plates, bolts and anchor braces, as shown in Figure 4. Once the infilled frame was fixed to the rigid frame, an OoP acceleration test was carried out using a rubber hammer to induce readings of OoP accelerations, which were measured at the center point of the wall. The data were obtained using a GY-61 ADXL335 triaxial accelerometer from Analog Devices™ connected to an Arduino Nano™ board. These measurements were further used to identify some of the OoP modal frequencies of the wall, as will be described in Section 2.4 below. After the OoP accelerations tests, the frame was released from its OoP restrains, whereupon an in-plane (IP) monotonic displacement-controlled loading test was carried out. In this step, a series of increasing horizontal loads were applied using an hydraulic jack to the top beam, and until the lateral drift was reached, followed by the unloading. In these loading and unloading sequences, the pair force vs deformation was measured using a MIRAN™ KTM Miniature pull rod displacement sensor with a nominal stroke of 200 mm, for the top beam displacements, and a pressure gauge directly installed in the hydraulic jack, for the applied forces. The steps described above were taken with increasing cycles of IP displacements to capture the IP degradation of the wall and its corresponding OoP modal frequencies during the degradation process. As mentioned in the previous section, the test was done on five one-quarter scale samples, due to limitations of the laboratory testing equipment. Additional test should be carried out to confer the method with better range of applicability; alternatively, in Section 6.2 a numerical model is developed and a parametric study is performed to overcome this limitation (see also Section 6.3).

2.3. In-plane measurements and characterization

The resulting measurements of IP pairs force vs displacement are shown in Figures 5 and 6, for the concrete and steel frames, respectively. Note that these figures also include (in solid line) the response of the concrete and steel bare frames, for comparison. Moreover, Figure 8(a) shows the secant IP stiffness in terms of the maximum deformation δ for each test, and also two tendency functions which describe the IP stiffness

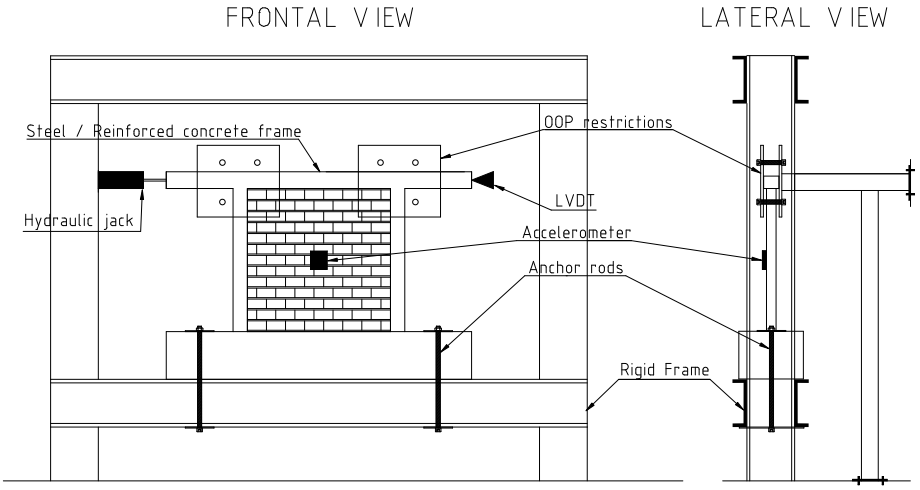

Figure 4: Layout of the experimental set-up required to obtain the in-plane and out-of-plane response data. The left side shows the frontal view, whereas the right side depicts the lateral view with indication of the anchor frame for out-of-plane restraint.

vs δ relation for the concrete (in dashed lines) and the steel frames (dot-dashed lines). These functions has been modelled using an exponential relation, as follows:

$$k_{IP} = Ae^{B\delta} + C \tag{3}$$

where A and B are uncertain model parameters which can be inferred through Bayesian inference, as shown further below, and C represents the initial stiffness of the frame without infills (in kN/mm). Similar tendencies on the stiffness degradation due to the maximum IP deformation have also been reported by other authors [15, 38, 50, 59, 65, 83, 92]. Besides, the tendencies observed in Figure 8(b) for the OoP fundamental frequency f_{OoP} vs δ (whose data will be described in the next section), also depict a similar exponential relation which can be described by the following equation:

$$f_{OoP} = De^{E\delta} - F \tag{4}$$

where D, E and F are uncertain model parameters.

These tests results indicate that an indirect inference of k_{IP} in terms of the f_{OoP}, is possible, as will be exposed in Section 3.

2.4. Out-of-plane measurements and characterization

As mentioned before, accelerations induced by an impulsive force applied perpendicularly to the mid point of the wall, were measured in a procedure similar to the experimental modal analysis method, but without an exact coincidence of the location of the applied force and the point of measurements [1]. The

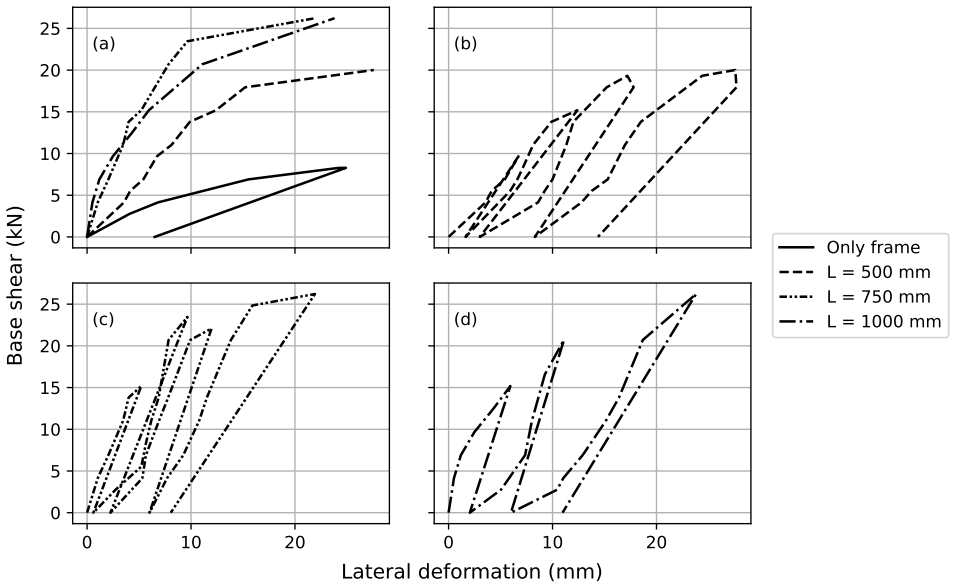

Figure 5: IP test results of the concrete frames. Panel (a): Envelopes of each test. Panels (b), (c) and (d): Load-Deformation history of the masonry infilled frames specimens.

OoPs accelerations were measured in different steps corresponding to incremental levels of deformation in the IP direction, as explained in the last section.

The recorded signals (i.e. each frame and each level of IP deformation) were subjected to a base-line correction and a band-pass filter with cut-off frequencies of 32 to 512 Hz. These cut-off frequencies were defined from an estimation made using a finite element structural model of the walls, where the higher cut-off frequency of 512 Hz was set as the maximum frequency value within the first five OoP vibration modes of the stiffest specimen.

To identify the natural frequencies of the specimens, a non-parametric identification procedure in the frequency domain [12] was used. This method, commonly referred to as frequency domain decomposition method, states that the dynamic response of a system can be obtained from a convolution, in the frequency domain, between the excitation signal and the response of an unitary impulse. The right panel of Figure 8 shows the results of the identified fundamental frequencies of all specimens in terms of the maximum lateral demand. Compared to the natural frequencies in Table 4, higher results were expected due to the reduced scale of the specimens. Note that the walls in Table 4 are walls from real buildings, while the specimens in this research were constructed with a reduced scale.

Then, the power density spectrum (PDS) is computed to obtain the energy level concentrated in each of the vibration frequencies. Figure 7 depicts the PDS of the steel frame specimen S500, per level of IP deformation. A moving average post-process was used to locate the maximum values of the PDS, along with a normalization to the maximum value. Notice that Table 4, which in general shows lower values of the

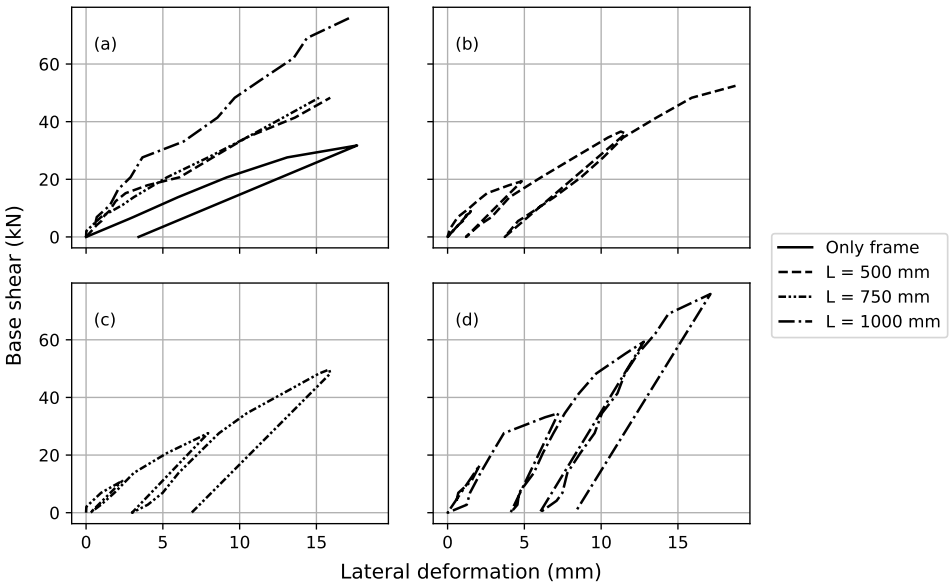

Figure 6: IP test results of the steel frames. Panel (a): Envelopes of each test. Panels (b) to (d): Load-Deformation history of the masonry infilled frames specimens.

measured frequency than the cases shown in Figure 8b, corresponds to real size walls and, due to their higher mass and lower stiffness, they result in a lower frequency than the one shown in Figure 7 and 8b. This was also confirmed with a dynamic linear model elaborated with shell-type elements, which was omitted herein to avoid deviating from the main theme of the article.

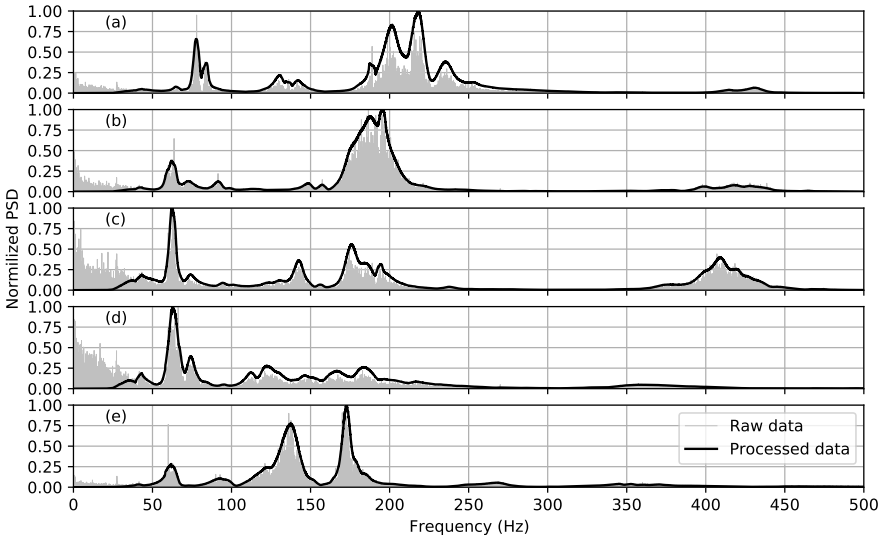

Figure 7: Power Density spectra of the OoP acceleration measurements of specimen S500 MIF. Panel (a): case undamaged. Panels (b) to (e) depict the results after each increasing IP deformation levels.

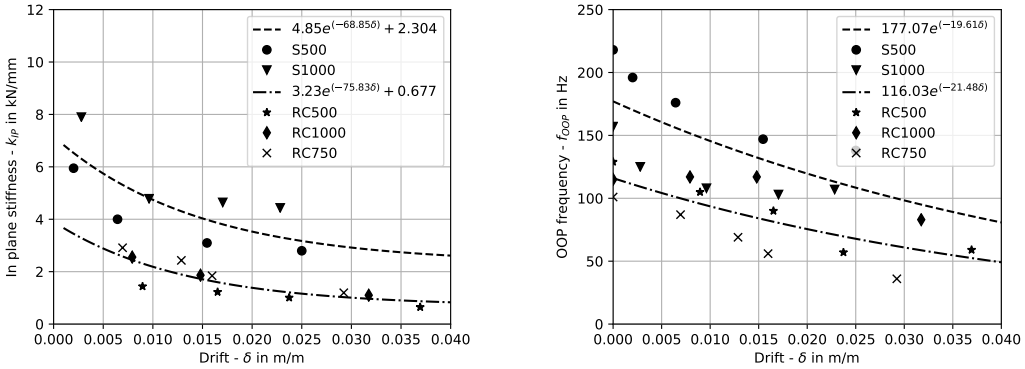

Figure 8: Degradation of IP stiffness (left) and reduction of OoP natural frequency (right) in terms of attained IP drift and type of frame.

3. Proposed MIF modelling approach

This section formulates the IP stiffness model based on the measured OoP fundamental frequency of the wall using a macro-modelling approach. The model is parameterized by a set of uncertain parameters, which are further inferred through Bayesian inference using the experimental data described in the previous section.

As stated before, a strut-based *macro-model* [82] has been adopted here to idealize the stiffening effect of the frame caused by the masonry infills. To this end, a 2D model was defined using OpenSeespy [91], which consisted of an *elastic truss* element placed along the principal diagonal of the frame bay, as shown in Figure 9. The strut section of this truss element is modelled as $A_m = t_m w_m$, where t_m is the thickness of the wall and w_m is assumed as one-third of the length of the wall's diagonal. Note that the proposed model is for use on linear-elastic structural analysis methods, typically employed for design purposes. Therefore, the model response lies within the elastic range. For the stiffness k_{IP} of this strut, the exponential decay relations between the IP and OoP behaviour, observed and described in the previous section (recall Equations (3), (4), and Figure 8), are used. Indeed, note that according to these observations, both the IP stiffness and the OoP fundamental frequency decay with the increase of lateral IP deformation. To model this coupled decay, Equations (3) and (4) are rearranged as follows:

$$\delta = \ln\left(\frac{k_{IP} - C}{A}\right)\frac{1}{B} \tag{5}$$

$$\delta = \ln\left(\frac{f_{OoP} - F}{D}\right)\frac{1}{E} \tag{6}$$

Next, these equations can be combined to obtain the K_{IP} as a function of f_{OoP}, as follows:

$$k_{IP} = A\left(\frac{f_{OoP} - F}{D}\right)^{\frac{B}{E}} + C \tag{7}$$

Finally, with no loss of generality, the last equation is simplified using only three model parameters, now called as $\theta_1, \theta_2, \theta_3$, leading to the following expression:

$$k_{IP} = \theta_1 \left(f_{OoP} - \theta_2\right)^{\theta_3} \tag{8}$$

In the last equation, the parameters θ_1 to θ_3 are uncertain parameters and can be inferred using the tests results, as described in the following section. Additionally, the strut macro-model considers two extra parameters to account for the concrete and steel stiffness. In total, five uncertain parameters comprise the proposed strut macro-model, namely $\boldsymbol{\theta} = \{\theta_1, ..., \theta_5\}$, where θ_1 to θ_3 are to consider the elastic modulus of the equivalent strut, based on the OoP fundamental frequency, θ_4 is a concrete frame stiffness modifier to consider the stiffness reduction due to cracking, and finally θ_5 is a steel frame stiffness modifier, to account for base plate rotational flexibility.

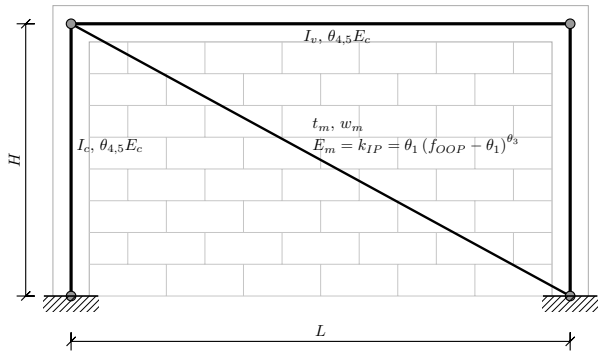

Figure 9: Elastic in plane macro model constructed in OpenSeespy.

4. Model inference through Approximate Bayesian Computation

The Equation 8 from the last section can be interpreted as a relation $g(\mathbf{u}, \boldsymbol{\theta}) : \mathbb{R}^{n_u} \times \mathbb{R}^{n_\theta} \rightarrow \mathbb{R}$ which provides a probabilistic output based on a set of input values $\mathbf{u} \in \mathbb{R}^{n_u}$, and also based on the uncertainty about the set of uncertain model parameters $\boldsymbol{\theta} \in \boldsymbol{\Theta} \subset \mathbb{R}^{n_\theta}$.

The initial quantification of the uncertainty about $\boldsymbol{\theta}$ is given by the *prior* probability density function (PDF) $p(\boldsymbol{\theta})$, which can be updated using the information in the dataset $\mathcal{D}$ through a *likelihood function* $p(\mathcal{D}|\boldsymbol{\theta})$, to obtain the posteior PDF $p(\boldsymbol{\theta}|\mathcal{D})$. From a mathematical point of view, the later can be obtained

through the Bayes's Theorem, as follows:

$$p\left(\boldsymbol{\theta}|\mathcal{D}\right) = \frac{p\left(\mathcal{D}|\boldsymbol{\theta}\right)p\left(\boldsymbol{\theta}\right)}{p\left(\mathcal{D}\right)} \tag{9}$$

where the term $p\left(\mathcal{D}|\boldsymbol{\theta}\right)$ is referred to as the *evidence* and represents how likely the data $\mathcal{D}$ are reproduced if model parametrized by $\boldsymbol{\theta}$ is adopted [10]. The approximate Bayesian computation (ABC) method [51] is an approach within the category of Bayesian inference and is used in those cases where the *likelihood function* is difficult, unknown, or analytically intractable to the Bayesian model updating approach. The ABC method produces samples of the pairs $(\theta, x) \in \mathcal{Z} \subseteq \boldsymbol{\Theta} \times \mathcal{D}$ which makes the model response $x = g(\boldsymbol{\theta}, \mathbf{u}) \sim p(x|\boldsymbol{\theta})p(\boldsymbol{\theta})$ lay within a defined region around the data $y \in \mathcal{D}$. In this work, x represents the output of the IP stiffness given by the Equation 8 and $p(x|\boldsymbol{\theta})$ the PDF of the IP stiffness values given $\boldsymbol{\theta}$. This region can be formally defined as:

$$\mathcal{N}_\epsilon(y) = \left\{x \in \mathcal{D} : \rho\big(\eta(x), \eta(y)\big) \leqslant \epsilon\right\} \tag{10}$$

where $\rho(\cdot)$ is a metric function which evaluates how close the probabilistic model output $x \sim p(x|\boldsymbol{\theta})$ is to the data $y \in \mathcal{D}$. The term ϵ is a tolerance parameter, and $\eta(\cdot)$ is a summary statistic [26] which, if required, allows a weak comparison between x and y. The resulting posterior samples produce an approximation of the posterior PDF referred to as $p_\epsilon(\boldsymbol{\theta}, x|y)$, which can be mathematically described as $p_\epsilon(\boldsymbol{\theta}, x|y) = p\big(\boldsymbol{\theta}, x|x \in \mathcal{N}_\epsilon(y)\big)$ which assigns higher probability density values to the pairs $(\boldsymbol{\theta}, x) \in \mathcal{Z}$ that produce $\rho\big(\eta(x), \eta(y)\big) \leqslant \epsilon$. The reader is referred to [81] for an overview and tutorial of the ABC methods.

Among the ABC methods published in the literature, the so called Adaptive Approximate Bayesian computation by Subset Simulation, also referred to as $\mathcal{A}^2$*BC-SubSim* [8], which is an improved variant of the original ABC-SubSim algorithm by Chiachio et al. [18], has been adopted in this work for its computationally efficiency and efficacy. To avoid duplicating the literature for this technique but to provide a sufficient background about the referred inference method, the relevant details of the implemented $\mathcal{A}^2$*BC-SubSim* algorithm are provided in a schematic manner in Figure 10. In such implementation, the prior PDF $p(\boldsymbol{\theta})$ of model parameters $\boldsymbol{\theta} = \{\theta_1, \ldots, \theta_5\}$ are taken as unidimensional uniforms within the range of values indicated in the plots from Figure 12.The tolerance parameter was set to $\epsilon = 4.0$, and the amount of simulations $N_s = 15000$. Additionally, the metric $\rho(\cdot)$ was defined as a relative $\mathbb{L}_1$-norm between the predicted and measured model output, namely:

$$\rho = \sum_{i=1}^{N} \left[\frac{\left| k_{IP}^{Model} - k_{IP(i)}^{Test} \right|}{k_{IP(i)}^{Test}} \right]_i \tag{11}$$

where $i = \{1, \ldots, N\}$ denotes the tests within the experimental campaign, k_{IP}^{Model} is the model simulation of the IP stiffness, and $k_{IP(i)}^{Test}$ is the measured IP stiffness, as per the i-test within the dataset $\mathcal{D}$. Note that k_{IP}^{Model} and $k_{IP(i)}^{Test}$ coincide with x and y respectively, as described in the Bayesian method given above.

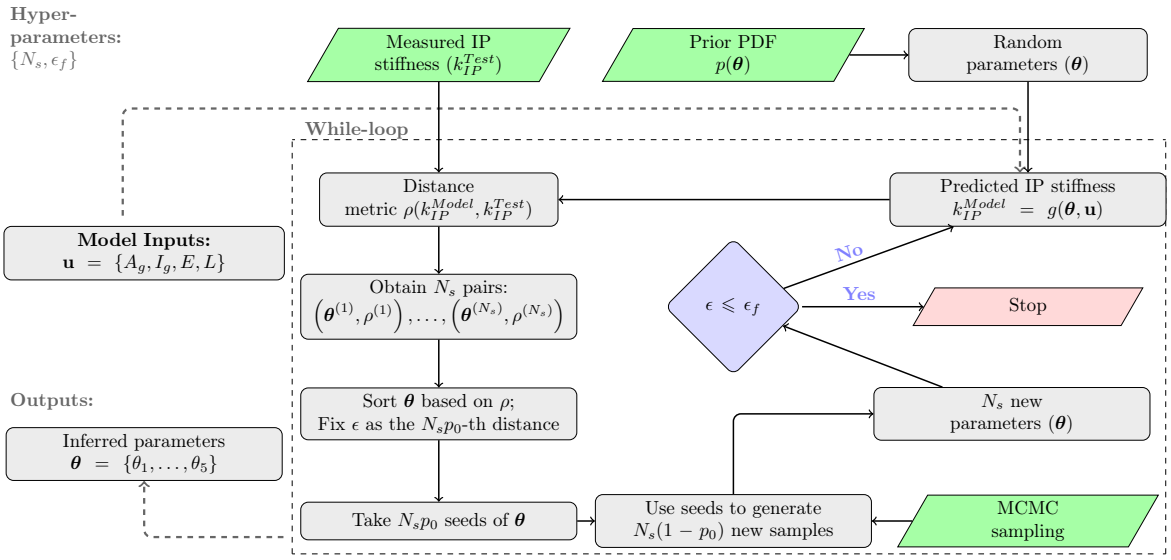

Figure 10: A flowchaining explaining $\mathcal{A}^2$BC-SubSim, Barros et al. [8]. $\tilde{\boldsymbol{\theta}}$ parameters are defined as the modifiers of Equation (8). A_g, I_g, E, L are the gross area, gross inertia, elastic modulus and length of the beam-column elements of the frame, respectively.

5. Results

The results of the inferred IP stiffness model based on measured OoP frequency are given in Figure 11. This figure gives comparison of the simulated model response obtained through simulating the model (recall Eq.8) using the posterior PDF of model parameters $p_\epsilon(\boldsymbol{\theta}, x|y)$, in contrast to the measured stiffness from the laboratory tests. These results demonstrate the plausibility to infer the IP stiffness of a masonry infilled frame by identifying the OoP fundamental frequency, and using Equation (8).

Additionally, Figure 12 depicts the *prior* and the *posterior* distribution of the inferred model parameters $\boldsymbol{\theta} = \{\theta_1, \ldots, \theta_5\}$. These plots indicate the regions of plausible values of $\boldsymbol{\theta}$ which make the data $\mathcal{D}$ better reproducible under the model parameterized by $\boldsymbol{\theta}$. In this figure, the plots in increasing gray tones indicate subsets of simulation which are explored by the $\mathcal{A}^2$BC-SubSim algorithm until the final posterior region (the darkest one) is reached.

6. Discussion

The results presented above demonstrated that obtaininig the IP stiffness of a MIF is possible by using the OoP frecuency measured through a non-destructive test. However, these results have been obtained after Bayesian learning of the model in Equation (8) using the set of data from the experimental campaing. Thus, the resulting model response is valid within the parameter range observed in such experimental data $\mathcal{D}$ used to learn the model parameters $\boldsymbol{\theta}$. This means that, those MIF cases whose configurations (i.e., lenght-to-high ratios, type of masonry, etc.) are not covered within the learning set $\mathcal{D}$, cannot be reliably

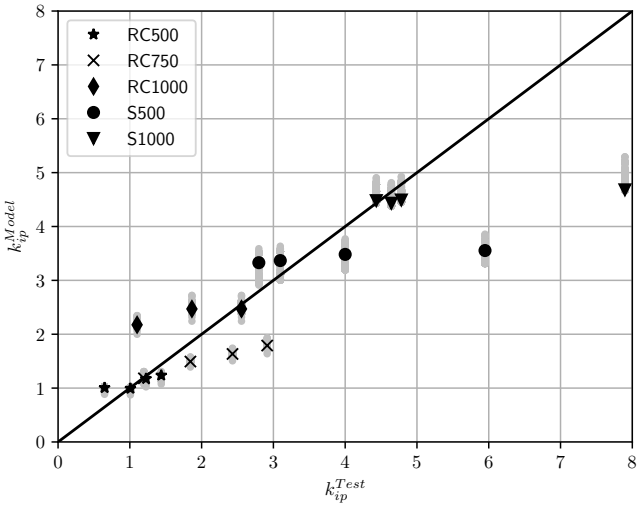

Figure 11: Comparison of the inferred model K_{IP} prediction, against the measured test results. Black marks correspond to the maximum a posteriori (MAP) estimation. Silver marks depict the range of the posterior distribution that results from the Bayesian analysis.

predicted. Increasing the experimental data until covering all possible parametric configurations of a MIF, would be an option, however, it seems economically infeasible and unpractical. An alternative, is to employ a meso-model based approach to investigate the influence of a number of MIF configuration parameters in the IP-OoP behaviour interaction. The resulting senstitivity study is further used to proposed an extended model of IP stiffness vs experimental OoP frecuency, which is tested in a number of simulated study cases.

6.1. Meso-model for MIF parametric study

The application of the *meso*-model called *Multi Pier*, recently proposed by Pirsaheb et al. [73], is explored and adapted to our dataset, because of the ease of its implementation in any software. The term *meso*-model refers to simulate the masonry units and mortar stress-strain behaviour as a merged element leading to a continuum material. Accordingly, the masonry wall is modelled with an equivalent 3D truss, allowing to directly consider the IP-OoP interaction of the masonry wall. Notice that the 3D truss model allows to consider either isotropic or anisotropic behaviour of any material, depending on the parameters employed for the struts in each main directions and/or diagonals. The *Multi Pier* model has the advantages of being computationally cheap, robust and easily implementable in most structural analysis software. On the other hand, its geometry is difficult to define, making it unpractical for large model applications.

In this work, the MIF meso-model has been built in OpenSeespy [91] and consists of two main parts: (1) the frame model and (2) the masonry wall model. Both parts are joined together using equal degree of freedom constraints, therefore assuming a perfect bond between the frame and the masonry wall. Figure 13 shows the bottom left 3D view of the MIF model geometry. It is worth mentioninig here that, due to the

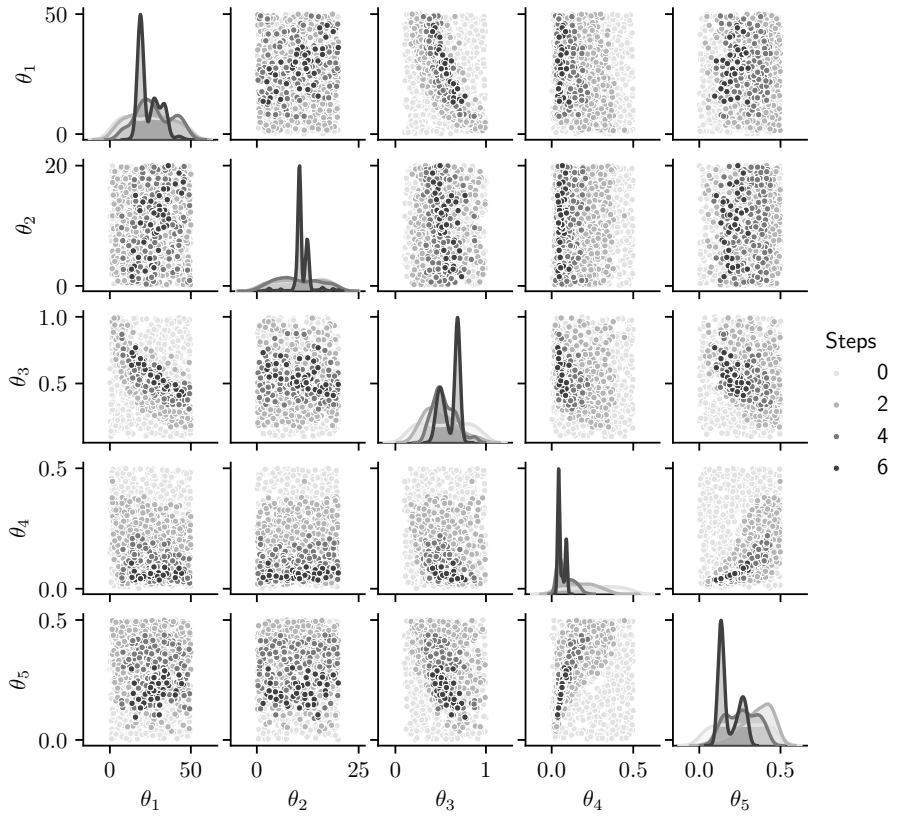

Figure 12: Scatter plot representation of the posterior PDF of $\Theta = \theta_1, ..., \theta_5$ as $\mathcal{A}^2$BC-SubSim output. The diagonal shows the kernel density estimates of the marginal posterior PDFs of each parameter of the simplified model of Section 3 .

aformentioned perfect bond assumption, the frame part of the meso-scale model can be either modelled as reinforced concrete or structural steel, since only its stiffness value in the OoP direction influences the model response. Therefore, with no loss of generality, the frame part was modelled as reinforced concrete in all cases.

Thus, the reinforced concrete frame model consists of distributed plasticity displacement-based beam-column elements with uni-axial constitutive models by a fiber section. OpenSees *Concrete01* and *Steel02* constitutive models were adopted to model the concrete and steel reinforcement behaviour, respectively. Parameter values were evaluated from the equations proposed by Karthik and Mander [41]. Strain penetration effects were also considered by means of a rotational spring at the base of the column. The parameters of the rotational spring were calibrated according to the bare frame test results (see Figure 5(a) and Section 2.1). The rotational spring was defined by a *Zero-Length* element and the *Hysteretic* constitutive model. Table 6 shows the parameter values of the fiber section and the rotational spring after the calibration process.

For the second part of the model (i.e. the masonry wall), a 3D truss composed by horizontal, vertical and diagonal elements with uni-axial behaviour, according to Pirsaheb et al. [73] recommendations, was used. *Concrete02* constitutive model was selected for every truss. The maximum compressive strength was set

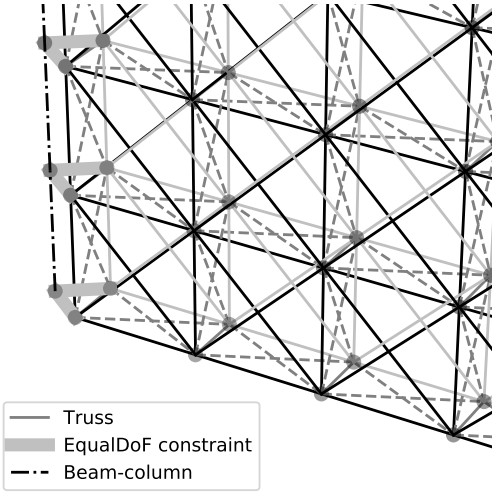

Figure 13: Isometric view of the bottom left part of the MIF model implemented in OpenSeespy.

to the characteristic compressive strength of the masonry (see Table 5). Notice that the characteristics of the material are defined in terms of stress and strain; however, truss models require an input in terms of force and deformation. The formulation applied for that conversion is described in detail by the original authors of the model, and the interested reader is referred to Pirsaheb et al. [73] for additional details. The model was calibrated to the force-displacement test results of the RC750 specimen shown in Section 2, referred to as the *original* model. The tensile strength of the masonry struts was assumed equal to the 5% of the compressive strength. The compressive strain at maximum strength was set equal to 0.2%. Then, the calibrated parameters of the aforementioned model were adapted to the RC500 and RC1000 specimens. Figure 14 shows the force-displacement response of the three type of specimens and their corresponding tests results. Table 7 gives a comparison of the prediction capabilities of the model about the OoP fundamental frequencies with respect to the measured ones. These results indicate that the meso-scale model is representative of the behaviour of the MIF structural system.

In the next section, the calibrated meso-model is used to study the influence of geometric and material parameters on the IP-OoP behaviour. Followed by a parametric study, a number of influencing coeficients to Equation 8, are obtained to extend the applicability of the proposed method in Section 3 to a wider range of possible cases. Irrespectively, the model has the following limitations which are highlighted here for clarity:

- The model does not directly consider the possibility of shear failure in the frame, because no shear model has been considered. Note also that, for the objective of the present study, it is not necessary to incorporate this behaviour.

- The model has only been calibrated for reinforced concrete frames with hollow concrete masonry infills. For other materials, a similar methodology should be followed, using appropriate laboratory test results.

Table 6: Parameter values of frame model.

Hysteretic - Zero-Length element

θ_1^{rot}	M_1	θ_2^{rot}	M_2
0.01008	1.52	0.32215	13.05
$Pinch_x$	$Pinch_y$	D_1	D_2
0.06200	0.29760	0.24010	0.12173
β			
0.26799			

Concrete01

f_c	ϵ_0	f_{cu}	ϵ_u
-20.0	-0.00200	-5.00	-0.01000

Steel02

f_y	E_s	b
500.0	200.00	0.140

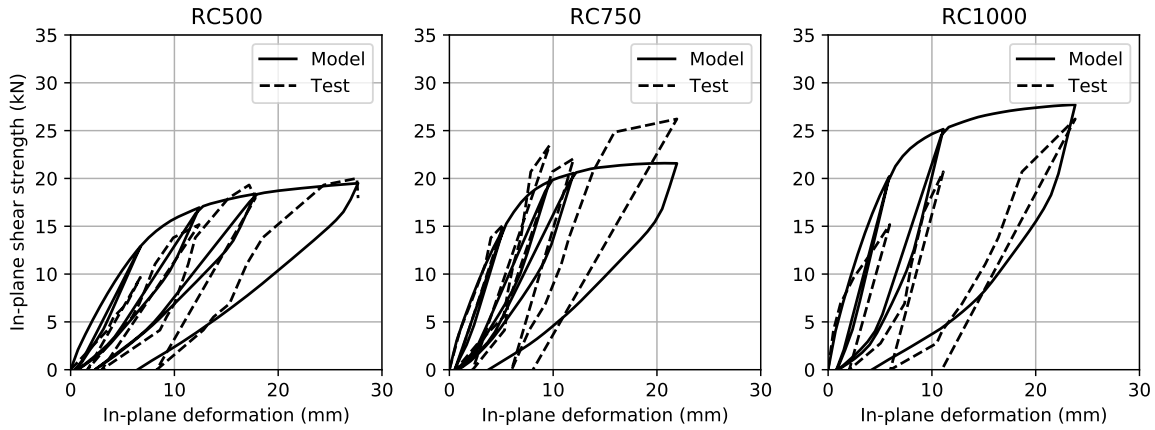

Figure 14: Comparison of the calibrated model estimation against the laboratory test results.

- A perfect bond between the frame and the wall has been assumed and, therefore, the results obtained for long and/or high walls should be used with caution, since in these cases the joint between the wall and the frame play an important role.

6.2. Parametric study

In this section, the influence of the following parameters in the interaction between IP stiffness and OoP fundamental frequency is studied, namely: masonry height-length ratio, masonry height-thickness ratio, masonry characteristic strength and geometric scale. As indicated before, the *original* model is set to be equal to the RC750 specimen with the following characterictics: $f_m = 1.0$ MPa, $t_m = 50$ mm, $L_m = 750$ mm and $H_m = 750$ mm, where f_m is the characteristic compressive strength of the masonry wall, and t_m, H_m, and L_m are the thickness, height and length of the wall, respectively.

Table 7: OoP fundamental frequency comparison between Multi Pier model and laboratory test measurement.

OoP test	Model			Measured			Error (%)		
	RC500	RC750	RC1000	RC500	RC750	RC1000	RC500	RC750	RC1000
1	150	102	85	129	101	115	16.3	1.0	26.1
2	128	81	63	105	87	117	21.9	6.9	46.2
3	91	79	62	90	69	117	1.1	14.5	47.0
4	79	73	48	57	56	83	38.6	30.4	42.2
5	79	73		59	36		33.9	102.8	

This parametric study first considers the influence of $^{H_m}/_{L_m}$ ratio by the definition of several L_m cases, as shown in Figure 15(a). Observe that the OoP fundamental frequency of the wall decreases with incresing deformation in any case. Figure 15(b) reveals that the increasing relation between OoP fundamental frequency and the $^{H_m}/_{L_m}$ ratio when the IP drift equals 0, follows a logaritmic tendency. However, this tendency is not clear for the RC1000 case, as per the measured results shown in Figure 8. This might be caused by the fact that the joint between the wall and the upper beam of the frame is usually difficult to construct properly, meaning that the perfect bond assumption may not be representative for the upper joint in that case. To address this issue, additional and dedicated tests would be required and, as a consequence, it is considered out of the scope of this work.

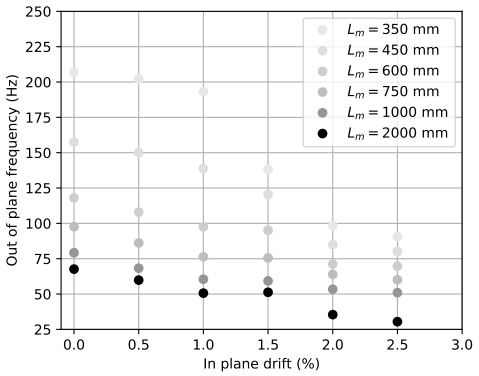

(a) Influence of masonry wall length and IP drift on the OoP frequency.

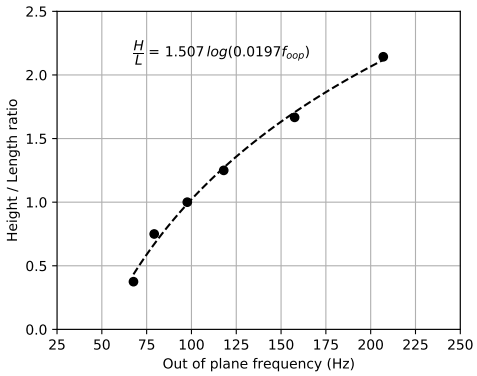

(b) Height-length ratio in terms of the measured OoP fundamental frequency for an undeformed MIF.

Figure 15: Influence of masonry height / length ratio on the IP and OoP stiffness.

Second, the $^{H_m}/_{t_m}$ influencing ratio is studied by adopting different t_m values, as shown in Figure 16(a). Observe again that the OoP fundamental frequency decays with the increase of the IP drift. Figure 16(b) shows the decreasing relationship between OoP fundamental frequency and the $^{H_m}/_{t_m}$ ratio, which follows a tendency that can be modelled by a cuadratic relation.

Next, the influence of f_m is explored by adopting a number of typical values, as shown in Figure 17(a). The results show that the OoP fundamental frequency decays with increasing IP drift. Also, Figure 17(b)

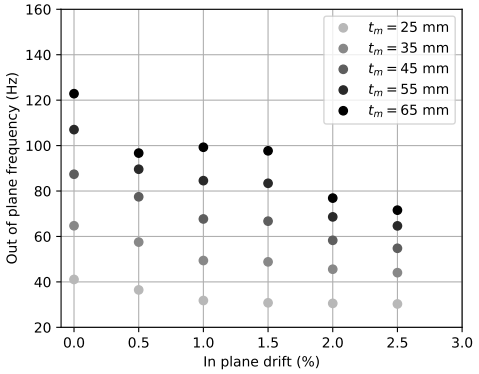

(a) Influence of masonry thickness and IP drift on the OoP frequency.

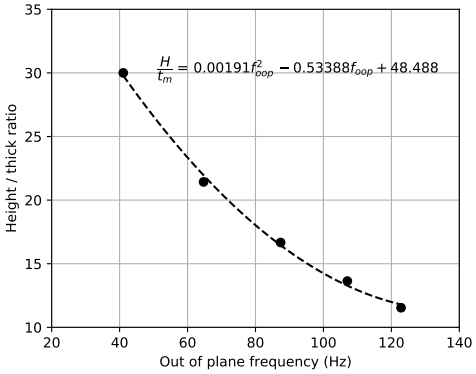

(b) Height-thickness ratio in terms of the measured OoP fundamental frequency for an undeformed MIF.

Figure 16: Influence of masonry height / thickness ratio on the IP and OoP stiffness

reveals an increasing relationship between OoP fundamental frequency with the f_m values, following a cuadratic tendency.

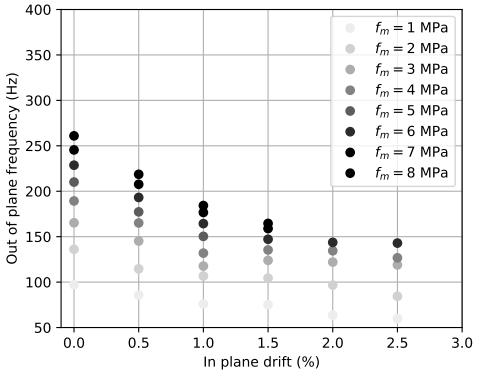

(a) Influence of masonry characteristic strength and IP drift on the OoP frequency.

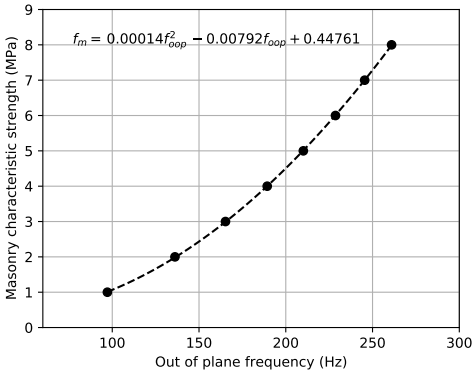

(b) Characteristic compressive strength in terms of the measured OoP fundamental frequency for an undeformed MIF.

Figure 17: Influence of the characteristic compressive strength of the masonry on the IP and OoP stiffness.

Finally, the influence of the size of the wall is investigated by means of a scaling factor. Figure 18(a) depicts similar tendency of decaying OoP fundamental frequency as the IP drift increases. And Figure 18(b) disclose a decreasing relationship between OoP fundamental frequency and the size scaling factor, which again, can be modelled by a cuadratic relation.

These observations are used in the following section to propose an extension to the model given by Equation 8, by means of a series of influencing coeficients.

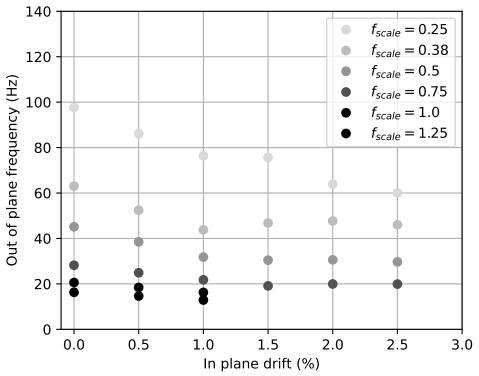

(a) Influence of scaling and IP drift on the OoP frequency.

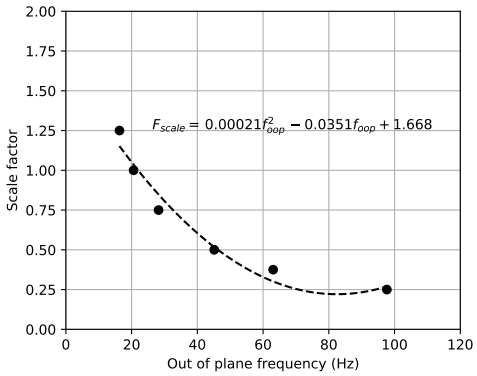

(b) Scaling factor in terms of the measured OoP fundamental frequency for an undeformed MIF.

Figure 18: Influence of the scaling factor of the masonry on the IP and OoP stiffness.

6.3. Extended MIF modelling approach

This section describes a method to extend the proposed model to estimate the IP stiffness of MIFs in terms of measured OoP fundamental frequency along with a number of configuration input parameters. This configuration input parameters allow the consideration of the influence of height, length, thickness, strength and scaling of the masonry wall. To this end, the Equation (8) is extended as follows:

$$k_{IP} = \theta_1 \left(f_{OoP} - \theta_2\right)^{\theta_3} \cdot f_{H/L} \cdot f_{H/t} \cdot f_{f'_m} \cdot f_{scale} \tag{12}$$

where the factors $f_{H/L}$, $f_{H/t}$, $f_{f'_m}$ and f_{scale} are modifier (or influencing) factors of the stiffness of the simplified strut model that account for height/length ratio, height/thickness ratio, the strength of the wall and the scaling factor (i.e. size of the wall), respectively.

These influencing factors were obtained from the results of the parametric study, using the following process:

1. For each model, the IP secant stiffness was obtained for the different levels of drift and different values of the parameters (i.e. length, thickness and strength).
2. The stiffness was normalized to the obtained stiffness of a basic case, corresponding to the values of the parameters of the *original* model. Figure 19 shows the relations that can be used to define the values of each influencing factors in terms of the MIF configuration parameters.

   Note that the limitations of the model used for the parametric study (see section 6.1), should also be considered in the results obtained with the proposed model.

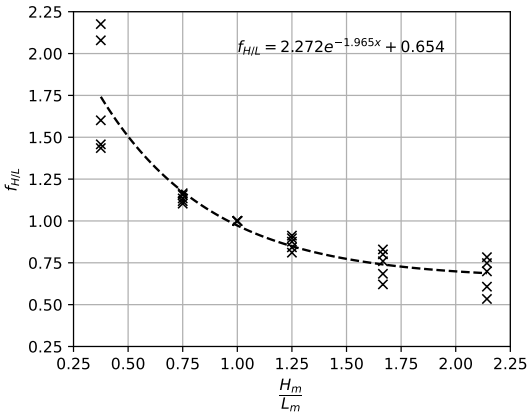

(a) Height-Length ratio modifier.

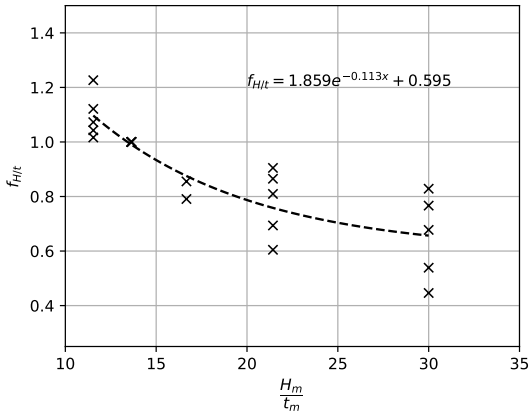

(b) Height-thickness ratio modifier.

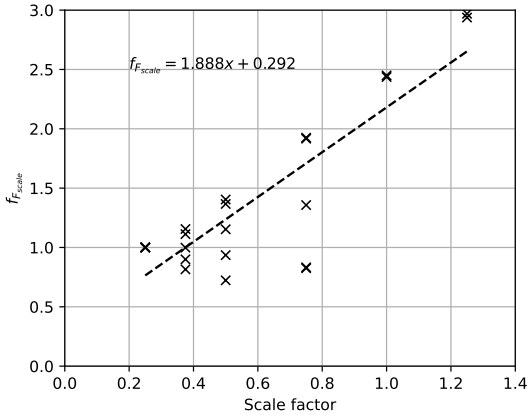

(c) Scaling factor modifier.

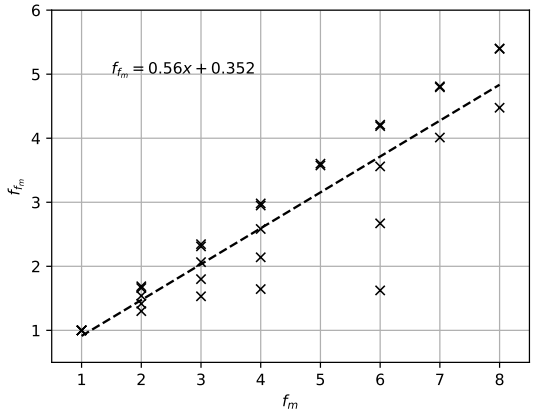

(d) Characteristic compressive strength modifier.

Figure 19: Functions of the modifier factors in terms of each influencing parameter.

6.3.1. Application examples

In this section, four additional models are considered to check the effectiveness of the proposed extended method defined by Equation (12) and Figures 19(a) to 19(d). The predictions given by the proposed extended model are compared to those given by the the Multi Pier MIF models described in Section 6.1. The geometric characteristics of each MIF cases are presented in Table 8. The table also shows the OoP fundamental frequency and the IP tangent stiffness of the MIF, obtained by the Multi-Pier numerical model. Finally, the influencing factors and the estimation of IP stiffness of the proposed method are presented. Also, the estimation obtained from available macro-models from the literature are presented at the bottom of the table for comparison purposes. This results are also presented in Figure 20. The MIF cases studied in this section were selected with the following criteria:

1. All cases are real size MIF structures. Notice that the scale factor shown in the table are defined

between 0.83 and 1.00. Those values are obtained considering that a 0.25 scale corresponds to a wall height equal to 750 mm.

2. Columns and beam sizes are defined equal for cases 1 and 2, and 3 and 4, respectively. Typical sizes for low-rise structures were adopted.
3. Case 1 represents a tall wall, i.e its length is smaller than the height. Case 2 is a short wall, where the length is higher than the height. Cases 3 and 4 represent the case of squared walls.
4. Cases 1 and 2 have a small height-to-thickness ratio, whilst cases 3 and 4 consider a higher value.
5. Cases 1 to 3 use walls with characteristic masonry strength equal to 1.00 MPa (and equal to the ones that were tested), whilst case 4 considers a higher strength value.

The results presented in Table 8 assume non-degraded MIFs defined using the Multi Pier methodology. Notice that the estimation of the secant stiffness of the macro models from the literature are close to the estimation obtained with the methodology proposed herein, whilst the tangent estimation is, in general, considerably larger than the results obtained from the proposed method. To consider some damage in the infills, the MIF were modelled with a relative deformation less than 1.00% of the height, and the results are shown in Table 9. Note that the models available in the literature are not able to estimate the stiffness of existing walls that have been subjected to IP deformation cycles. For this reason, the proposed methodology has the advantage over existing macro-models in that the estimation is based on field measurement and, thus, is able to consider the deformation history of the wall.

As shown in Table 8, satisfactory predictions were obtained for the case of non-degraded MIFs, showing a mistmach between the Multi-Pier model and the proposed extended simplified model of 4%, 15%, 25%, and 34% for each case, respectively. For the degraded MIFs simulations, differences of 70%, 25%, 38% and 5%, were observed for cases 1 to 4, respectively. These results indicate that the proposed methodology can be considered as a practical tool for the stiffness evaluation of existing MIF structures, and also to quantify its uncertainty. However, it is recommended that, before its application in real cases, the calibration of the method should be improved with a larger set of laboratory tests, in order to study the influence of other variables such as: type and material of the masonry units, characteristics of the mortar, the bond between the wall and the frame, among others.

Table 8: Summary of results of application examples for non-degraded MIFs from Section 6.3.1.

	Parameter	Case 1	Case 2	Case 3	Case 4
Frame sections	Column (mm)	400x400	400x400	300x300	300x300
	Beam (mm)	300x400	300x400	250x350	250x350
Wall geometry	L_m (mm)	2000	4000	3000	3000
	H_m (mm)	2500	2500	3000	3000
	t_m (mm)	200	200	150	150
	f_m (MPa)	1.00	1.00	1.00	5.00
	H_m/L_m	1.25	0.63	1.00	1.00
	H_m/t_m	12.50	12.50	20.00	20.00
	Scale factor	0.83	0.83	1.00	1.00
Multi Pier model	f_{OoP} (Hz)	44.6	29.1	17.6	38.4
	k_{IP} (kN/mm)	15.4	29.7	8.9	41.2
Geometric modifiers	$f_{H/L}$	0.90	1.25	1.00	1.00
	$f_{H/t}$	1.05	1.05	0.78	0.78
	f_{scale}	1.95	1.95	2.20	2.20
	f_m	1.00	1.00	1.00	3.20
Simplified model	k_{IP}^{mean} (kN/mm)	16.0	25.4	6.7	27.2
	k_{IP}^{std} (kN/mm)	1.30	1.91	1.17	1.22
[37]	k_{IP}^{sec} (kN/mm)	17.84	33.07	12.82	64.10
[46]		15.68	29.42	10.99	37.50
[77]		17.50	17.64	11.37	56.85
[37]	k_{IP}^{tan} (kN/mm)	29.63	63.34	30.99	83.80
[46]		38.37	72.00	26.89	91.77
[77]		90.00	180.00	84.38	421.88

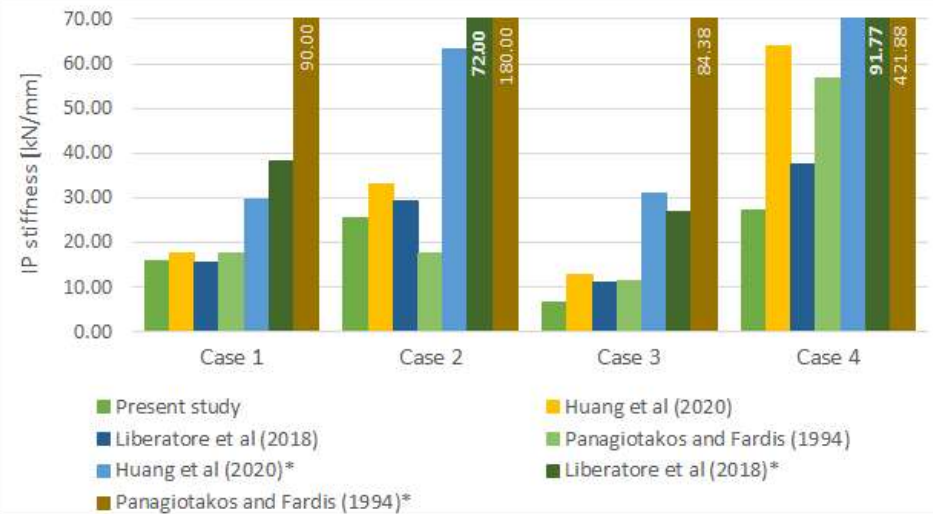

Figure 20: Stiffness estimation of infilled masonry case studies using the formulations of Table 1. The sign * refers to tangent stiffness estimation.

Table 9: Summary of results of application examples for degraded MIFs from Section 6.3.1.

	Parameter	Case 1	Case 2	Case 3	Case 4
Multi Pier model	f_{OoP} (Hz)	26.44	20.5	13.5	27.8
	k_{IP} (kN/mm)	7.3	15.9	4.7	22.2
Simplified model	k_{IP}^{mean} (kN/mm)	12.5	20.0	2.9	21.1
	k_{IP}^{std} (kN/mm)	1.95	2.73	0.60	0.80

7. Conclusions

This paper proposed a methodology to indirectly infer the IP stiffness of MIFs by means of the OoP fundamental frequency that can be measured through a low-cost non-destructive test. Using an experimental campaign of five one-fourth scaled MIFs, a simplified model was proposed and inferred to the data to indirectly predict the IP stiffness based on the identified OoP fundamental frequency. The applicability of the method was further extended to properly cover model predictions out-of the configuration range given by the experimental data, by means of a parametric study performed with a MIF physics-based meso-model. Influencing coefficients were obtained to consider the effects of height-length ratio, height-thickness ratio, the masonry characteristic strength and the scale size of the MIF. A number of application examples were presented, demonstrating the capability and adequacy to predict the IP stiffness of MIFs from their OoP fundamental frequencies.

To the authors' knowledge, this is the first time that such methodology has been proposed to estimate the stiffness contribution of existing masonry infilled frame structures. The method is able to consider the effects of the degradation due to the not known history of deformations to which the existing wall may had been subjected to. This feature of the method allows for better stiffness estimation compared to existing macro-model formulations, making it a suitable tool for the evaluation of existing structures. However, the proposed method requires additional laboratory testing to confirm the results obtained here by numerical modelling and to better capture the influence of different damage scenarios of the masonry walls to the MIF structural system. Thus, desirable future work includes a larger scale MIF structure tested on a shake table with consideration of varying frame-wall bond condition, among others.

Acknowledgements

This work was supported by the SINDE (Research and Development System of the Catholic University of Santiago de Guayaquil - UCSG, Ecuador) under project code 491/170, which provided funding for the UGR-UCSG Permenant Research Seminar in Civil Engineering. The authors would like to thank the ENHAnCE ITN project (`https://www.h2020-enhanceitn.eu/`) funded by the European Union's Horizon 2020 research and innovation programme under the Marie Skłodowska-Curie grant agreement No. 859957.

The authors gratefully acknowledge the support of these organisations which have enabled the research reported in this paper. The authors also acknowledge the operational support provided by Carlos Alberto Vargas and personel of the CEINVES Structural Laboratory at UCSG during the conduct of the laboratory tests.

Bibliography

[1] Allemang, R. J. (1983). Experimental modal analysis. *NASA Technical reports*.

[2] Alwashali, H., Sen, D., Maeda, M., Monical, J., Sikder, M., and Islam, M. (2019). Study on Seismic Capacity of Existing Rc Buildings With Masonry Infill Based on Past Earthquakes Damage. *2019 Pacific Conference on Earthquake Engineering*, 41(2):1015–1020.

[3] Angel, R., Abrams, D. P., Shapiro, D., Uzarski, J., and Webster, M. (1994a). Behavior of reinforced concrete frames with masonry infills. *Civil Engineering Studies SRS-589*.

[4] Angel, R., Shapiro, D., Uzarski, J., and Webster, M. (1994b). Behavior of Reinforced Concrete Frames With Masonry Infills. *Civil Engineering Studies*, 16509(589):183.

[5] Argudo, J., Arellano, M., Villacrés, A., and Mera, W. (1999). Proyecto radius - herramientas de evaluación del riesgo para el diagnóstico de zonas urbanas contra desastres sísmicos. Technical Report 1, Facultad de ingeniería - Universidad Católica de Santiago de Guayaquil, Guayaquil - Ecuador.

[6] ASCE/SEI 41 (2017). *Seismic Evaluation and Retrofit of Existing Buildings*. American Society of Civil Engineers, ASCE/SEI 41-17 edition.

[7] Bahreini, V., Mahdi, T., and Najafizadeh, M. (2017). Numerical Study on the In-Plane and Out-of-Plane Resistance of Brick Masonry Infill Panels in Steel Frames. *Shock and Vibration*, 2017:1–16.

[8] Barros, J., Chiachío, M., Chiachío, J., and Cabanilla, F. (2021). Adaptive approximate bayesian computation by subset simulation for structural model calibration. *Computer-Aided Civil and Infrastructure Engineering*, 37(6):726–745.

[9] Bashandy, T., Rubiano, N. R., and Klingner, R. E. (1991). *Evaluation and analytical verification of infilled frame test data*. Phil M. Ferguson Structural Engineering Laboratory, University of Texas at Austin.

[10] Beck, J. L. (2010). Bayesian system identification based on probability logic. *Structural Control and Health Monitoring*, 17(7):825–847.

[11] Bennett, R. M., Boyd, K. A., and Flanagan, R. D. (1997). Compressive properties of structural clay tile prisms. *Journal of Structural Engineering*, 123(7):920–926.

[12] Brincker, R., Zhang, L., and Andersen, P. (2000). Output-only modal analysis by frequency domain decomposition. In *Proceedings of ISMA25: 2000 International Conference on Noise and Vibration Engineering*, pages 717–723. Katholieke Universiteit, Leuven.

[13] Brodsky, A., Rabinovitch, O., and Yankelevsky, D. Z. (2018). Effect of masonry joints on the behavior of infilled frames. *Construction and Building Materials*, 189.

[14] Butenweg, C., Marinković, M., and Salatić, R. (2019). Experimental results of reinforced concrete frames with masonry infills under combined quasi-static in-plane and out-of-plane seismic loading. *Bulletin of Earthquake Engineering*, 17(6):3397–3422.

[15] Cai, G. and Su, Q. (2019). Effect of Infills on Seismic Performance of Reinforced Concrete Frame structures—A Full-Scale Experimental Study. *Journal of Earthquake Engineering*, 23(9):1–29.

[16] Calvi, G. M. and Bolognini, D. (2001). Seismic response of reinforced concrete frames infilled with weakly reinforced masonry panels. *Journal of Earthquake Engineering*, 05(02):153–185.

[17] Cavaleri, L., Zizzo, M., and Asteris, P. G. (2020). Residual out-of-plane capacity of infills damaged by in-plane cyclic loads. *Engineering Structures*, 209(December 2018):109957.

[18] Chiachio, M., Beck, J., Chiachio, J., and Rus, G. (2014). Approximate Bayesian Computation by Subset Simulation. *SIAM Journal of Scientific Computing*, 36:A1339–A1358.

[19] Dawe, J. and Seah, C. (1989). Out-of-plane resistance of concrete masonry infilled panels. *Canadian Journal of Civil Engineering*, 16(6):854–864.

[20] De Angelis, A. and Pecce, M. R. (2018). Out-of-plane structural identification of a masonry infill wall inside beam-column RC frames. *Engineering Structures*, 173(June):546–558.

[21] De Risi, M. T., Di Domenico, M., Ricci, P., Verderame, G. M., and Manfredi, G. (2019). Experimental investigation on the influence of the aspect ratio on the in-plane/out-of-plane interaction for masonry infills in rc frames. *Engineering Structures*, 189:523–540.

[22] Di Domenico, M., De Risi, M. T., Ricci, P., Verderame, G. M., and Manfredi, G. (2021). Empirical prediction of the in-plane/out-of-plane interaction effects in clay brick unreinforced masonry infill walls. *Engineering Structures*, 227(January 2020):111438.

[23] Di Trapani, F., Bertagnoli, G., Ferrotto, M. F., and Gino, D. (2018). Empirical equations for the direct definition of stress–strain laws for fiber-section-based macromodeling of infilled frames. *Journal of Engineering Mechanics*, 144(11):04018101.

[24] Di Trapani, F., Tomaselli, G., Vizzino, A., and Bertagnoli, G. (2021). Assessment of out-of-plane strength of masonry infills through a FE augmented dataset. *Procedia Structural Integrity*, 33(C):896–906.

[25] Drysdale, R. G. and Essawy, A. S. (1988). Out-of-plane bending of concrete block walls. *Journal of Structural Engineering*, 114(1):121–133.

[26] Fearnhead, P. and Prangle, D. (2012). Constructing summary statistics for approximate Bayesian computation: Semi-automatic approximate Bayesian computation. *Journal of the Royal Statistical Society: Series B (Statistical Methodology)*, 74(3):419–474.

[27] Ferretti, F., Ferracuti, B., Mazzotti, C., and Savoia, M. (2019). Destructive and minor destructive tests on masonry buildings: Experimental results and comparison between shear failure criteria. *Construction and Building Materials*, 199:12–29.

[28] Furtado, A., Rodrigues, H., Arêde, A., and Varum, H. (2016). Experimental evaluation of out-of-plane capacity of masonry infill walls. *Engineering Structures*, 111:48–63.

[29] Furtado, A., Rodrigues, H., Arêde, A., and Varum, H. (2017). Modal identification of infill masonry walls with different characteristics. *Engineering Structures*, 145:118–134.

[30] Griffith, M. C., Lam, N. T., Wilson, J. L., and Doherty, K. (2004). Experimental investigation of unreinforced brick masonry walls in flexure. *Journal of Structural Engineering*, 130(3):423–432.

[31] Haseltine, B. (1976). Design of laterally loaded wall panels. In *Proceedings of the British Ceramic Society*, pages 115–126, Stoke-on-Trent. British Ceramic Society.

[32] Haseltine, B., West, H., and Tutt, J. (1977). Design of walls to resist lateral loads. *Structural engineer*, 55(10):422–430.

[33] Hashemi, A. and Mosalam, K. M. (2006). Shake-table experiment on reinforced concrete structure containing masonry infill wall. *Earthquake engineering & structural dynamics*, 35(14):1827–1852.

[34] Hashemi, S. A. (2007). *Seismic evaluation of reinforced concrete buildings including effects of masonry infill walls*. University of California, Berkeley.

[35] Hendry, A. (1973). The lateral strength of unreinforced brickwork. *Structural Engineer*, 2(51):43–50.

[36] Hendry, A. and Kheir, A. (1976). The lateral strength of certain brickwork panels. In *Proceedings of the fourth international brick masonry conference*, Brugee, Belgium.

[37] Huang, H., Burton, H. V., and Sattar, S. (2020). Development and Utilization of a Database of Infilled Frame Experiments for Numerical Modeling. *Journal of Structural Engineering (United States)*, 146(6).

[38] Jiang, H., Liu, X., and Mao, J. (2015). Full-scale experimental study on masonry infilled RC moment-resisting frames under cyclic loads. *Engineering Structures*, 91:70–84.

[39] Kadysiewski, S. and Mosalam, K. (2009). Modeling of unreinforced masonry infill walls considering in-plane and out-of-plane interaction, peer 2008/102. *University of California, Berkeley*, 144.

[40] Kam, W. Y., Pampanin, S., Dhakal, R., Gavin, H. P., and Roeder, C. (2010). Seismic performance of reinforced concrete buildings in the september 2010 darfield (canterbury) earthquake. *Bulletin of the New Zealand Society for Earthquake Engineering*, 43(4):340–350.

[41] Karthik, M. M. and Mander, J. B. (2011). Stress-block parameters for unconfined and confined concrete based on a unified stress-strain model. *Journal of Structural Engineering*, pages 270–273.

[42] Kaushik, H. B., Rai, D. C., and Jain, S. K. (2006). Code approaches to seismic design of masonry-infilled reinforced concrete frames: A state-of-the-art review. *Earthquake Spectra*, 22(4):961–983.

[43] Klingner, R., Rubiano, N., Bashandy, T. R., and Sweeney, S. (1996). Evaluation and analytical verification of shaking table data from infilled frames. *Part*, 2:521–532.

[44] Kong, J., Zhai, C., and Wang, X. (2016). In-plane behavior of masonry infill wall considering out-of-plane loading. *Periodica Polytechnica Civil Engineering*, 60(2).

[45] Lefter, J. and Colville, J. (1974). Reinforcing existing buildings to resist earthquake forces. In *U.S. National Conference of Earthquake Engineering*, Ann Arbor, Oakland.

[46] Liberatore, L., Noto, F., Mollaioli, F., and Franchin, P. (2018). In-plane response of masonry infill walls: Comprehensive experimentally-based equivalent strut model for deterministic and probabilistic analysis. *Engineering Structures*, 167:533–548.

[47] Lourenço, P. (1997). *Computational strategies for masonry structures*. PhD thesis, Delft University.

[48] Lourenço, P. B., Milani, G., Tralli, A., and Zucchini, A. (2007). Analysis of masonry structures: review of and recent trends in homogenization techniques. *Canadian Journal of Civil Engineering*, 34(11):1443–1457.

[49] Lubliner, J., Oliver, J., Oller, S., and Oñate, E. (1989). A plastic-damage model for concrete. *International Journal of solids and structures*, 25(3):299–326.

[50] Mansouri, A., Marefat, M. S., and Khanmohammadi, M. (2014). Experimental evaluation of seismic performance of low-shear strength masonry infills with openings in reinforced concrete frames with deficient seismic details. *The Structural Design of Tall and Special Buildings*, 23(15):1190–1210.

[51] Marjoram, P., Molitor, J., Plagnol, V., and Tavare, S. (2003). Markov chain Monte Carlo without likelihoods. *Proceedings of the National Academy of Sciences*, 100(26):15324–15328.

[52] Mazzotti, C., Sassoni, E., and Pagliai, G. (2014). Determination of shear strength of historic masonries by moderately destructive testing of masonry cores. *Construction and Building Materials*, 54:421–431.

[53] McDowell, E., McKee, K., and Sevin, E. (1956). Arching action theory of masonry walls. *Journal of the Structural Division*, 82(2):915–1.

[54] McDowell, E., McKee, K., and Sevin, E. (1957). Dicsussion of "arching action theory of masonry walls". *Journal of the Structural Division*, 83(1):1156–9.

[55] Milanesi, R. R., Kurukulasuriya, M., Bolognini, D., Grottoli, L., Dacarro, F., and Morandi, P. (2023). Experimental investigation of seismic behaviour of existing masonry infills. In *2nd Croatian Conference on Earthquake Engineering – 2CroCEE*, pages 148–159. University of Zagreb Faculty of Civil Engineering.

[56] Milanesi, R. R., Morandi, P., Dacarro, F., Albanesi, L., and Magenes, G. (2017). In-plane cyclic and out-of-plane dynamic testing procedures for infilled RC frames. In *International Conference on Advances in Experimental Structural Engineering*, volume 2017-Septe, pages 243–261.

[57] Milijaš, A., Marinković, M., Butenweg, C., and Klinkel, S. (2023a). Experimental results of reinforced concrete frames with masonry infills with and without openings under combined quasi-static in-plane and out-of-plane seismic loading. *Bulletin of Earthquake Engineering*, 21(7):3537–3579.

[58] Milijaš, A., Šakić, B., Marinković, M., Butenweg, C., Gams, M., and Klinkel, S. (2023b). Behaviour of masonry infills with

door openings under sequential in-plane and out-of-plane loading. In *2nd Croatian Conference on Earthquake Engineering – 2CroCEE*, pages 160–169, Zagreb. University of Zagreb Faculty of Civil Engineering.

[59] Misir, I. S., Ozcelik, O., Girgin, S. C., and Yucel, U. (2016). The Behavior of Infill Walls in RC Frames Under Combined Bidirectional Loading. *Journal of Earthquake Engineering*, 20(4):559–586.

[60] Mohamed, H. and Romão, X. (2021). Robust Calibration of Macro-Models for the In-Plane Behavior of Masonry Infilled RC Frames. *Journal of Earthquake Engineering*, 25(3):407–433.

[61] Mohammad Noh, N., Liberatore, L., Mollaioli, F., and Tesfamariam, S. (2017). Modelling of masonry infilled RC frames subjected to cyclic loads: State of the art review and modelling with OpenSees. *Engineering Structures*, 150:599–621.

[62] Mohyeddin, A., Goldsworthy, H. M., and Gad, E. F. (2013). Fe modelling of rc frames with masonry infill panels under in-plane and out-of-plane loading. *Engineering Structures*, 51:73–87.

[63] Monk, C. (1958). *Resistance of structural clay masonry to dynamic forces*. Structural Clay Products Research Foundation.

[64] Morandi, P., Hak, S., and Magenes, G. (2013). Simplified out-of-plane resistance verification for slender clay masonry infills in rc frames. *Proceedings of the XV ANIDIS, L'Ingegneria Sismica in Italia, Padua, Italy*, 30.

[65] Morandi, P., Hak, S., and Magenes, G. (2018). Performance-based interpretation of in-plane cyclic tests on RC frames with strong masonry infills. *Engineering Structures*, 156:503–521.

[66] Mosalam, K. and Günay, S. (2015). Progressive collapse analysis of rc frames with urm infill walls considering in-plane/out-of-plane interaction. *Earthquake Spectra*, 31(2):921–943.

[67] Nasiri, E. and Liu, Y. (2019). The out-of-plane behaviour of concrete masonry infills bounded by reinforced concrete frames. *Engineering Structures*, 184:406–420.

[68] Nasiri, E. and Liu, Y. (2020). Effect of prior in-plane damage on the out-of-plane performance of concrete masonry infills. *Engineering Structures*, 222(July).

[69] Nicoletti, V., Arezzo, D., Carbonari, S., and Gara, F. (2020). Expeditious methodology for the estimation of infill masonry wall stiffness through in-situ dynamic tests. *Construction and Building Materials*, 262:120807.

[70] Nicoletti, V., Gara, F., Regni, M., Carbonari, S., and Dezi, L. (2018). Dynamic in situ tests for the calibration of an infilled R.C. Building F.E. model. *EESMS 2018 - Environmental, Energy, and Structural Monitoring Systems, Proceedings*, pages 1–6.

[71] Palieraki, V., Zeris, C., Vintzileou, E., and Adami, C. E. (2018). In-plane and out-of plane response of currently constructed masonry infills. *Engineering Structures*, 177(December 2017):103–116.

[72] Paulay, T. and Priestley, M. N. (1992). *Seismic design of reinforced concrete and masonry buildings*, volume 768. Wiley New York.

[73] Pirsaheb, H., Javad Moradi, M., and Milani, G. (2020). A Multi-Pier MP method for the non-linear static analysis of out-of-plane loaded masonry walls. *Engineering Structures*, 223(November 2019):111040.

[74] Reynders, E. (2012). System Identification Methods for (Operational) Modal Analysis: Review and Comparison. *Archives of Computational Methods in Engineering*, 19(1):51–124.

[75] Ricci, P., Di Domenico, M., and Verderame, G. M. (2018a). Experimental assessment of the in-plane/out-of-plane interaction in unreinforced masonry infill walls. *Engineering Structures*, 173:960–978.

[76] Ricci, P., Di Domenico, M., and Verderame, G. M. (2018b). Experimental investigation of the influence of slenderness ratio and of the in-plane/out-of-plane interaction on the out-of-plane strength of URM infill walls. *Construction and Building Materials*, 191:507–522.

[77] Sassun, K., Sullivan, T. J., Morandi, P., and Cardone, D. (2016). Characterising the in-plane seismic performance of infill masonry. *Bulletin of the New Zealand Society for Earthquake Engineering*, 49(1):98–115.

[78] Sattar, S. and Liel, A. B. (2016a). Seismic performance of nonductile reinforced concrete frames with masonry infill walls - I: Development of a strut model enhanced by finite element models. *Earthquake Spectra*, 32(2):795–818.

582 [79] Sattar, S. and Liel, A. B. (2016b). Seismic performance of nonductile reinforced concrete frames with masonry infill walls -
583 II: Collapse assessment. *Earthquake Spectra*, 32(2):819–842.
584 [80] Sezen, H., Elwood, K., Whittaker, A., Mosalam, K., Wallace, J., and Stanton, J. (2000). *Structural Engineering*
585 *Reconnaissance of the Kocaeli (Izmit): Turkey Earthquake of August 17, 1999*. Pacific Earthquake Engineering Research
586 Center.
587 [81] Sisson, S. A., Fan, Y., and Beaumont, M. (2018). *Handbook of approximate Bayesian computation*. CRC Press.
588 [82] Tarque, N., Candido, L., Camata, G., and Spacone, E. (2015). Masonry infilled frame structures: state-of-the-art review of
589 numerical modelling. *Earthquakes and Structures*, 8(3):733–759.
590 [83] Tasnimi, A. A. and Mohebkhah, A. (2011). Investigation on the behavior of brick-infilled steel frames with openings,
591 experimental and analytical approaches. *Engineering Structures*, 33(3):968–980.
592 [84] Thomas, F. (1953). The strength of brickwork. *The Structural Engineer*, 31(2):35–46.
593 [85] Timoshenko, S. and Woinowsky-Krieger, S. (1959). *Theory of plates and shells*, volume 1. McGraw-Hill, second edition.
594 [86] Urich, A. J. and Beauperthuy, J. L. (2012). Protagonism of the Infill Walls on Seismic Performance of Venezuela Buildings.
595 *15th World Conference on Earthquake Engineering (15WCEE)*.
596 [87] Varum, H., Furtado, A., Rodrigues, H., Dias-Oliveira, J., Vila-Pouca, N., and Arêde, A. (2017). Seismic performance
597 of the infill masonry walls and ambient vibration tests after the Ghorka 2015, Nepal earthquake. *Bulletin of Earthquake*
598 *Engineering*, 15(3):1185–1212.
599 [88] Villalobos, E., Sim, C., Smith-Pardo, J. P., Rojas, P., Pujol, S., and Kreger, M. E. (2018). The 16 April 2016 Ecuador
600 earthquake damage assessment survey. *Earthquake Spectra*, 34(3):1201–1217.
601 [89] West, H., Hodgkinson, H., and Webb, W. (1973). Lateral loading tests on walls with different boundary conditions. In
602 *Proceedings of the Third International Brick Masonry Conference (Essen) 1973, eds L. Foertig and K. Gobel (Bundesverband*
603 *der Deutschen Ziegelindustrie, Bonn, 1975)*, pages 180–6.
604 [90] Yuen, Y. P. and Kuang, J. S. (2014). Masonry-infilled RC frames subjected to combined in-plane and out-of-plane loading.
605 *International Journal of Structural Stability and Dynamics*, 14(02):1350066.
606 [91] Zhu, M., McKenna, F., and Scott, M. H. (2018). Openseespy: Python library for the opensees finite element framework.
607 *SoftwareX*, 7:6–11.
608 [92] Zovkic, J., Sigmund, V., and Guljas, I. (2013). Cyclic testing of a single bay reinforced concrete frames with various types
609 of masonry infill. *Earthquake Engineering & Structural Dynamics*, 42(8):1131–1149.